

On the polymorphism of benzocaine; a low-temperature structural phase transition for form (II)

Eric J. Chan,* A. David Rae and
T. Richard Welberry

Research School of Chemistry, Australian
National University, Canberra, ACT 0200,
Australia

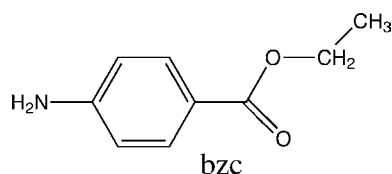
Correspondence e-mail: echanj@rsc.anu.edu.au

Received 18 March 2009
Accepted 19 May 2009

A low-temperature structural phase transition has been observed for form (II) of benzocaine (BZC). Lowering the temperature doubles the *b*-axis repeat and changes the space group from $P2_12_12_1$ to $P112_1$ with γ now 99.37° . The structure is twinned, the twin rule corresponding to a 2_1 screw rotation parallel to **a**. The phase transition is associated with a sequential displacement parallel to **a** of zigzag bi-layers of ribbons perpendicular to **b***. No similar phase transition was observed for form (I) and this was attributed to the different packing symmetries of the two room-temperature polymorphic forms.

1. Introduction

Benzocaine (BZC) and other similarly structured local anaesthetic drugs (Schmidt, 2005*b*) are of substantial importance to the pharmaceutical industry. Crystal polymorphism is often found to occur and the structural interpretations of the associated changes in behavioural characteristics use a variety of analytical procedures and are often centred around powder diffraction (Gruno *et al.*, 1993; Schmidt, 2005*a*). Previous single-crystal X-ray diffraction studies revealed two forms for BZC, form (I) crystallizing as monoclinic $P2_1/c$ (Lynch & McClenaghan, 2002), with $\beta = 91.699(4)^\circ$ (our results), form (II) as orthorhombic (Sinha & Pattabhi, 1987) $P2_12_12_1$. The latter two reports also indicate great similarities in the intermolecular stacking of the two forms. The difference between the two forms is in the nature of the flat ribbons of structure that propagate along the **a** direction. These ribbons consist of two symmetry-related halves. The first half is essentially the same for both ribbons, *i.e.* molecules separated by the lattice repeat *a* with the methyl atoms in the centre of the ribbon and the amine atoms on the outside of the ribbon. Methyl groups of symmetry-related molecules are spaced $1/2a$ apart along the centre of the ribbon. A ribbon is propagated by inversion centres in form (I), but a 2_1 screw axis in form (II), see Fig. 1. Layers of ribbons perpendicular to **c*** have adjacent ribbons related by an inversion in form (I), but a 2_1 screw axis parallel to **a** in form (II). As a consequence the outsides of such a layer of ribbons are essentially the same, *i.e.* molecules are related by translation only, but are either inversion-related [form (I)] or 2_1 screw-related [form (II)]. Adjacent layers of ribbons perpendicular to **c*** are related by a 2_1 screw axis parallel to **b**, and this creates chains of hydrogen bonding that are essentially identical for both forms.



Recently a new phase has been found, form (III), which arises from a low-temperature (150 K) structural phase transition of form (II). However, no low-temperature structural phase transition is observed for form (I). The phase transition results in a twinned structure with the new cell having the *b* axis doubled and the now monoclinic $P112_1$ structure having $\gamma = 99.370(2)^\circ$. The phase transition is associated with a sequential displacement parallel to **a** of zigzag bi-layers of ribbons perpendicular to **b***. The phase transition was also recently shown to be related to elongated diffuse scattering features parallel to **b*** in form (II). Fig. 6 from previous literature (Chan *et al.*, 2009) highlights the key differences in reciprocal space with respect to the BZC system and shows the direction of spot splitting for twin-related reflections in form (III).

Our investigation of the crystalline BZC structural system includes an evaluation of re-collected single-crystal X-ray diffraction data at room temperature (300 K) for forms (I) and (II), and a structure determination for the low-temperature (150 K) dataset for form (III) using the same crystal as was used for form (II).

It should be noted that for ease of structural comparison we have used the same sequence of axial lengths for each structure and have chosen the origin of the $P2_12_12_1$ structure so as to make the atom positions for the asymmetric unit coincide. As a consequence, form (I) is in its standard setting whereas form (II) does not have the magnitudes of the axial lengths in the sequence smallest to largest, nor does it have the standard origin. The transformation from the standard setting is then

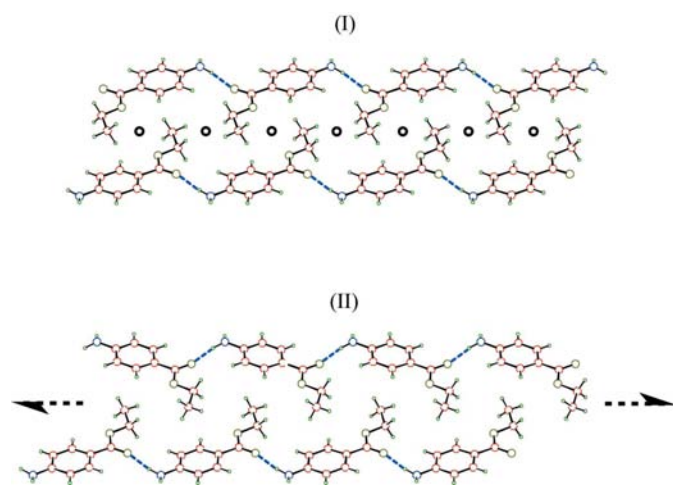


Figure 1

View down **b** of ribbon structures propagating along the *a* axis in the two room-temperature forms of BZC. The blue dashed lines represent the N–H...O hydrogen-bonding motif.

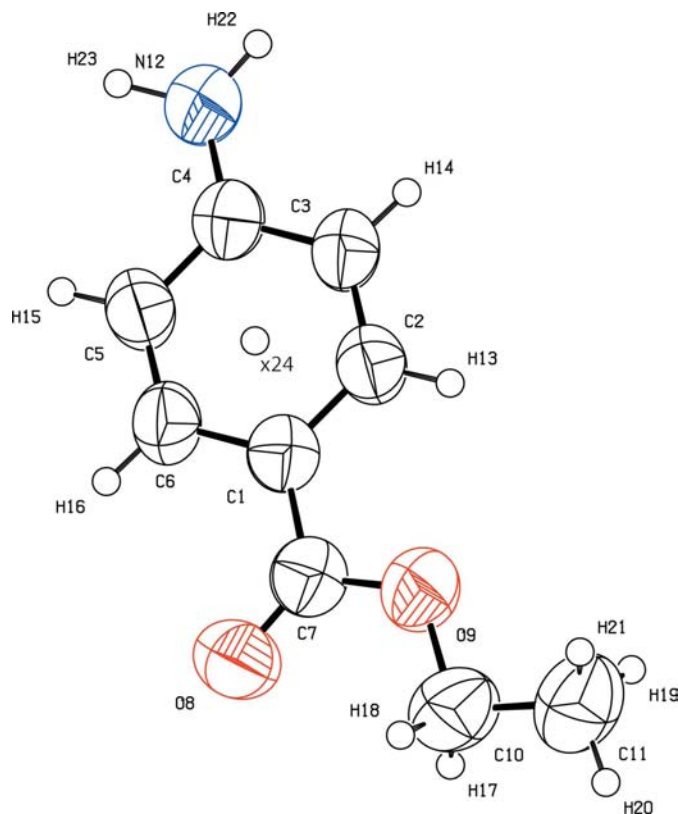


Figure 2

Labelled ORTEP diagram of form (I) of BZC as a representative of the molecule in all three polymorphic forms. 50% probability displacement ellipsoids are shown for non-H atoms. Centroid x24 has been calculated from the atom positions of the six-membered ring.

$x, y, z \Rightarrow -y + \frac{1}{4}, x, z + \frac{1}{4}$ giving equivalent positions x, y, z ; $-x, y + \frac{1}{2}, -z + \frac{1}{2}$; $x + \frac{1}{2}, -y, -z$; $-x + \frac{1}{2}, -y + \frac{1}{2}, z + \frac{1}{2}$. The cell for form (III) was also chosen to relate to form (I) and the structure was evaluated using equivalent positions x, y, z ; $-x, -y, z + \frac{1}{2}$ and an origin choice along **c**. The origin was moved along **b**, changing the equivalent positions to x, y, z ; $-x, -y + \frac{3}{4}, z + \frac{1}{2}$ to create the structures drawn in the figures. The deposited CIF file gives fractional coordinates for the equivalent positions substituted.¹

2. Experimental

2.1. Crystal growth

BZC 98% (ALDRICH) was used as a starting material. Suitable crystals of both polymorphic forms (I) and (II) were obtained by slow evaporation from ethanol solutions at room temperature.

2.2. Structure determinations

Full spheres of CCD area-detector X-ray data were collected using the area detector of an Enraf–Nonius kappaCCD diffractometer (ω scans, Mo $K\alpha$ radiation, $\lambda =$

¹ Supplementary data for this paper are available from the IUCr electronic archives (Reference: SO5027). Services for accessing these data are described at the back of the journal.

0.7107 Å) and ‘numerical’ absorption corrections (Coppens, 1970) were applied before data merging. The observed reflection data for the room-temperature forms (I) and (II) were used in the full-matrix least-squares refinement of F^2 in *SHELXL97* (Sheldrick, 2008), whereas those collected from the low-temperature form (III) were refined using the constrained least-squares refinement program *RAELS2006* (Rae, 2006). The twinning in form (III) was ignored in the data processing, reflection intensities being obtained using only reflection positions \mathbf{h} for the major twin component. The final twin ratio was 0.523 (2):0.477. The twinning was included in the model for observed intensities as $Y_{\text{calc}}(\mathbf{h}) = aI(\mathbf{h}) + (1-a)K(|\mathbf{h} - \mathbf{h}'|) I(\mathbf{h}')$, where $K(|\mathbf{h} - \mathbf{h}'|)$ is an empirical function allowing for overlap with the nearest twin-related

reflection \mathbf{h}' . $K(|\mathbf{h} - \mathbf{h}'|)$ is 0.5 if $p = |\mathbf{h} - \mathbf{h}'|$ is equal to a refinable parameter p_1 , 1.0 if less than a refinable parameter p_2 , 0.0 if greater than $2p_1 - p_2$ and $0.5 - 0.5 \sin[\pi(p - p_1)/2(p_1 - p_2)]$ for p in the range p_2 to $2p_1 - p_2$. The nearest twin-related reflection to h, k, l has $h' = h, l' = -l$ and k' the nearest integer to $-k - 0.42309h$. Final parameter values were $p_1 = 0.139$ (3) b^* and $p_2 = 0.0$. To demonstrate the adequacy of the twin-overlap model the reflection data considered observed were separated into eight sets, corresponding to $p = 0, 0 < p/b^* \leq 0.1, 0.1 < p/b^* \leq 0.2$ and $p/b^* > 0.2$ for k even (1–4) and k odd (5–8). For the 216, 299, 845, 1578, 210, 299, 869 and 1697 reflections in each set the final values for $R(F)$ were 0.063, 0.041, 0.082, 0.072, 0.059, 0.042, 0.080 and 0.057.

An original structure model for form (III) was obtained by starting the refinement using fractional coordinates implied by the structure of form (II). However, a false minimum was obtained corresponding to having kept the wrong half of the 2_1 screw axes parallel to c when doubling the b axis. However, it was clear that the ribbons of the structure were essentially unchanged. Packing arguments were then used to establish the final model that refined successfully. Adjacent layers of structure are related by pseudo- 2_1 screw rotations about axes parallel to \mathbf{b}^* . Three successive screw rotations are essentially the same as for form (II), but the fourth is relocated along \mathbf{a} creating the doubled b

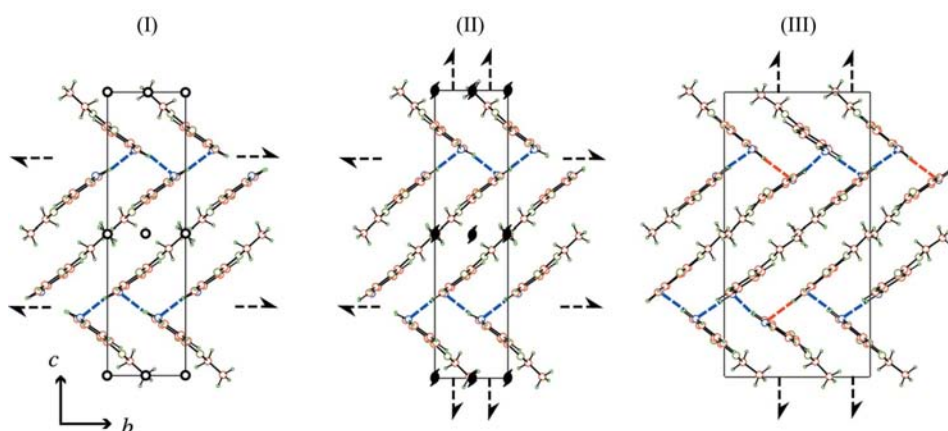


Figure 3

Individual plots down the a axis depict the major differences between the three forms of BZC. The blue dashed lines represent the $\text{N}-\text{H}\cdots\text{N}$ hydrogen-bonding motif which is broken when form (II) undergoes the phase transition to the low-temperature form (III), in which zigzag bi-layers of molecules slide relative to each other. The centre of such a bi-layer is the zigzag $x, \frac{3}{4}, -\frac{1}{4}$ to $x, -\frac{1}{4}, \frac{1}{4}$ to $x, \frac{3}{4}, \frac{3}{4}$ to $x, -\frac{1}{4}, \frac{5}{4}$. The instances where $\text{N}-\text{H}\cdots\text{N}$ contacts are substituted for $\text{N}-\text{H}\cdots\pi$ interactions are identified by red dashed lines.

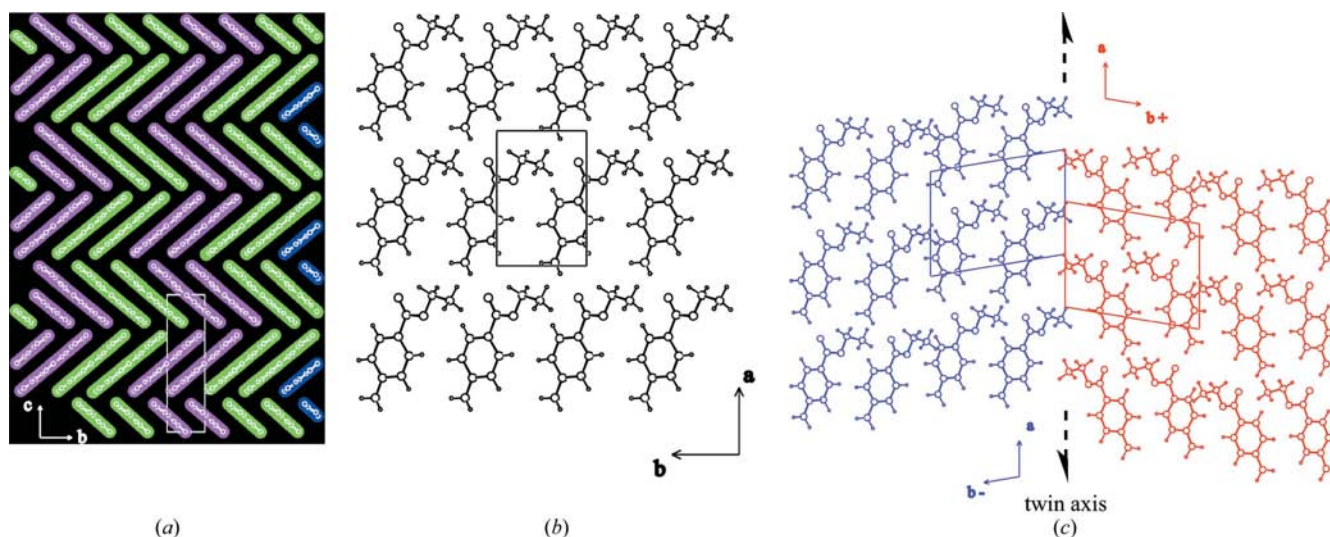


Figure 4

(a) Representation of zigzag bi-layers comprising ribbon-pair molecular motifs viewed down the a axis of the form (II) structure. (b) View of a single molecular layer projected down the c axis in form (II). (c) View of two single molecular layers projected down the c axis in form (III) that are related by a 2_1 screw acting as a twinning mechanism.

Table 1

Crystal data collection and refinement parameters for the three forms of BZC ($C_9H_{11}NO_2$, $M_r = 165.19$).

	Form (I)	Form (II)	Form (III)
Crystal data			
Chemical formula	$C_9H_{11}NO_2$	$C_9H_{11}NO_2$	$C_9H_{11}NO_2$
Crystal system, space group	Monoclinic, $P2_1/c$	Orthorhombic, $P2_12_12_1$	Monoclinic, $P112_1$
Temperature (K)	300	300	150
a, b, c (Å)	8.2570 (7), 5.5009 (4), 19.956 (2)	8.2424 (4), 5.3111 (3), 20.904 (1)	8.1883 (4), 10.6394 (5), 20.476 (1)
β, γ (°)	91.699 (4), 90	90, 90	90, 99.370(2)
V (Å ³)	906.0 (2)	915.12 (9)	1760.1 (2)
Z	4	4	8
Radiation type	Mo $K\alpha$	Mo $K\alpha$	Mo $K\alpha$
μ (mm ⁻¹)	0.09	0.09	0.09
Crystal form, size (mm)	Block, 0.15 × 0.15 × 0.07	Block, 0.28 × 0.24 × 0.17	Block, 0.28 × 0.24 × 0.07
Data collection			
Diffractometer	KappaCCD	KappaCCD	KappaCCD
Data collection method	CCD	CCD	CCD
Absorption correction	Integration	Integration	Integration
T_{min}	0.980	0.958	0.952
T_{max}	0.989	0.978	0.974
No. of measured, independent and observed reflections	12 216, 1595, 1108	20 874, 1241, 1003	24 960, 7859, 6013
Criterion for observed reflections	$I > 2\sigma(I)$	$I > 2\sigma(I)$	$I > 2\sigma(I)$
R_{int}	0.040	0.066	0.063
θ_{max} (°)	25.1	27.5	27.5
Refinement			
$R(F), R(F^2), S$	0.041, 0.122, 1.01	0.039, 0.112, 1.06	0.065, 0.098, 2.10
No. of reflections	1595	1241	6013
No. of parameters	153	117	143
H-atom treatment	Refined independently	Mixture of independent and constrained refinement	Constrained to parent site
$(\Delta/\sigma)_{max}$	< 0.0001	< 0.0001	< 0.01†
$\Delta\rho_{max}, \Delta\rho_{min}$ (e Å ⁻³)	0.12, -0.10	0.08, -0.08	0.12, -0.10

Computer programs used: *Collect* (Hoofdt, 2005), *HKL DENZO* and *SCALEPACK* (Otwinowski & Minor, 1997), *SHELXL97* (Sheldrick, 2008), *XTAL3.7* (Hall *et al.*, 2001), *RAELS2000* (Rae, 2006). † Refinement using TLX constraints usually converges to a stationary value of S with this sort of value for $(\Delta/\sigma)_{max}$, because large covariances between parameters are not taken into account.

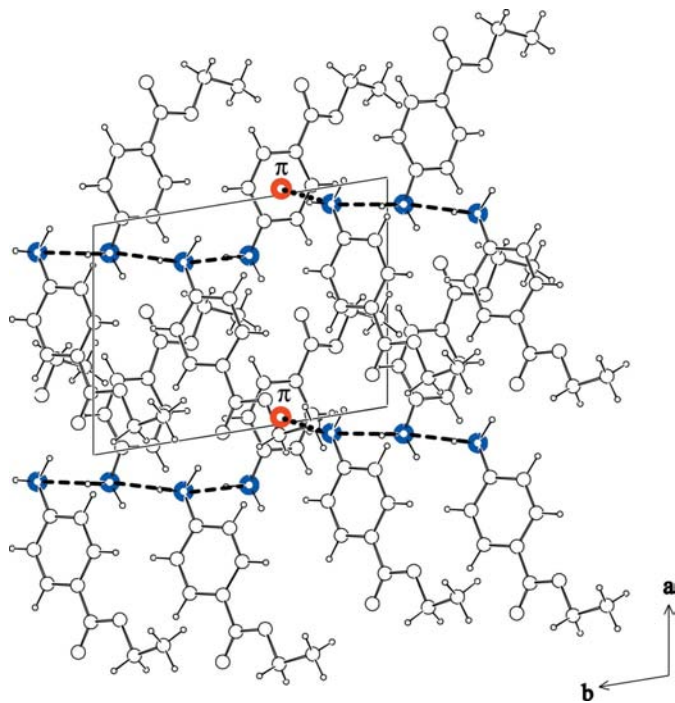


Figure 5

Projection down the c axis of two layers of form (III) of BZC showing the $N-H \cdots N$ interactions as dashed lines and $N-H \cdots \pi$ interactions as dotted lines. This figure is in colour in the electronic version of this paper.

axis and the change in γ . The asymmetric unit for form (III) contains four molecules compared with one for both (I) and (II). The projection of the structure down **a** is essentially the same for forms (I), (II) and (III), see Fig. 3.

For forms (I) and (II) all non-H atoms were refined as independent atoms with anisotropic displacement parameters using neutral atom-scattering curves corresponding to Table 2.2B of *International Tables for Crystallography* (Vol. C, 1995, pp. 500–501). For form (I) all H-atom positional and U_{iso} parameters were refined (initial locations calculated from neighbouring sites). For form (II) only the positions and U_{iso} values of those H atoms bound to N were refined, whereas those bound to C atoms were treated with a riding model where the U_{iso} was set equal to 1.2 or 1.5 (methyl group) times that of the parent atom. For form (III) the model included a limited number of constraints to achieve an anisotropic atom refinement. Refinable local coordinates defined relative to refinable local orthonormal axial systems were used to constrain the phenyl rings and their attached C and N to be planar and equal with the ring atoms having $mm2$ symmetry (Rae, 1975*a,b*). Rigid-body TLX parameterization was used to describe and refine the atomic displacement parameters of every atom in a molecule (Rae, 1975*a,b*). All other non-H atoms were refined as independent atoms with anisotropic displacement parameters. H atoms were reinserted in

Table 2

Internal coordinates for the three forms of BZC.

Form	(I)	(II)	(III) [†]
Bond distances (Å)			
Average phenyl C–phenyl C	1.385	1.384	1.393
Carboxyl C–O	1.338 (2)	1.334 (2)	1.348
Carbonyl C=O	1.209 (2)	1.210 (2)	1.214
Phenyl C–N	1.373 (2)	1.380 (2)	1.373 (2)
Ethyl C–C	1.487 (4)	1.480 (2)	1.498
Phenyl C–C	1.468 (2)	1.469 (2)	1.474 (2)
Ethyl C–O	1.450 (2)	1.455 (2)	1.453
Mean deviation from planarity for COOC ₂ H ₅ moiety (Å)	0.032 (2)	0.013 (3)	0.028 (2)
C ₆ H ₅ –COOC ₂ H ₅ inter-planar dihedral angle (°)	5.36 (5)	6.38 (6)	6.11 (4)

[†] Standard errors for average values are omitted. Constraints made some distances equal for four molecules in (III).

Table 3

Listing of hydrogen-bond distances (Å) for the three forms of BZC.

Form		(I)	(II)	(III) [†]	
				Type 1	Type 2
N12–H22···O8 ⁱ	D–H	0.86 (2)	0.92 (2)	1.00	
	H···A	2.10 (2)	2.05 (2)	1.99	
	D···A	2.956 (2)	2.946 (2)	2.947	
	D–H···A angle (°)	168 (2)	165 (2)	157	
N12–H23···N12 ⁱⁱ	D–H	0.91 (2)	0.97 (2)	1.00	1.00
	H···A	2.43 (2)	2.33 (2)	2.18	3.30
	D···A	3.316 (2)	3.265 (2)	3.180	4.094 (3)
	D–H···A angle (°)	165 (2)	162 (2)	173	143
N12–H23···π ^{iii‡}	D–H	0.91 (2)	0.97 (2)	1.00	1.00
	H···A	3.77 (2)	3.75 (2)	3.52	2.51
	D···A	4.300 (2)	4.285 (2)	4.171	3.423 (2)
	D–H···A angle (°)	120 (1)	118 (1)	125	152

Symmetry codes: for forms (I) and (II): (i) $x-1, y, z$; (ii) $-x, y-\frac{1}{2}, \frac{1}{2}-z$; form (III) involves non-equivalent molecules. [†] Type 1 refers to those molecules of the structure that have a coordination environment similar in magnitude to forms (I) and (II), whereas Type 2 is indicative of those regions of structure that have changed as a result of the phase transition (e.g. interaction between molecules 1 and 4 of the asymmetric unit). Average values have been used where appropriate. Standard errors are omitted whenever averages or calculated hydrogen positions are used. [‡] π is represented by the centroid position calculated from the atom positions of a six-membered ring.

geometrically sensible positions after each refinement cycle and given atomic displacement parameters determined by the parameters of the atoms to which they were attached.

Reflection weights were $[\sigma^2(F^2) + (w_1P)^2 + w_2P]^{-1}$, where $P = (F_o^2 + 2F_c^2)/3$ for those models refined on F^2 in *SHELX97*. Weights were $[\sigma^2(F) + (0.03F)^2]^{-1}$ for the refinement on F using *RAELS06*. Crystal data parameters unique to each model are summarized below in Table 1. Fig. 2 shows a molecule of form (I) with 50% probability amplitude displacement ellipsoids for the non-H atoms. H atoms, where shown, have an arbitrary radii of 0.1 Å (Hall *et al.*, 2001).

3. Results and discussion

Previous literature identifies two polymorphic forms for BZC at room temperature (Sinha & Pattabhi, 1987; Lynch & McClenaghan, 2002). A comparison of the molecular internal coordinates (Table 2) reveals inter-planar dihedral angles between ring and carboxyl groups consistent with the planar quinoid character, as previously indicated by Sinha (Sinha & Pattabhi, 1987), with carboxyl and ethyl moieties (COO₂CH₃) also showing little deviation from planarity between forms. Other internal parameters for all forms remain consistent, subtle elongations in average bond distances for the low-temperature form being attributed to a reduction in rotational disorder. No individual anisotropic displacement parameters deviate ominously from what would be expected, thus the molecule in all forms can be considered to be both rigid and planar. The success of the *TLX* modelling for form (III) confirms this observation.

In both structures strong end-on N–H···O hydrogen bonds are associated with the translation along the *a* axis. Planar ribbons along *a* are formed by using a symmetry element to interlock two such half ribbons, using either an inversion, form (I), or a 2₁ screw axis parallel to *a*, form (II). Layers of ribbons perpendicular to *c** relate adjacent ribbons by inversion in form (I) and by a 2₁ screw axis parallel to *a*, form (II). Adjacent layers are interconnected through chains of N–H···N hydrogen bonds propagated by 2₁ screw axes parallel to *b* creating a herringbone arrangement of ribbons when viewed down *a*.

If we now consider only the molecules immediately linked by these two forms of hydrogen bonding we create a hydrogen-bonded layer perpendicular to *c** that is essentially identical for both forms (I) and (II). The stacking difference between the room-temperature polymorphs is simply how the ethyl groups of either side of such a layer slot into each other at a 'hydrophobic interface'. These hydrogen-bonded layers are either related by an inversion centre, form (I), or a 2₁ screw axis parallel to *a*, form (II) (Fig. 3). As a result of this similarity of the packing for both room-temperature forms there are few differences in the connectivity between them (Table 3), the main differences being associated with what can be considered to be the 'hydrophobic interface'. This is a feature exploited in previous studies (see Table 3 of Chan *et al.*, 2009, for a list of the differences).

The 2₁ screw axis parallel to *c* is the only symmetry operation which is preserved during the reversible phase transition that changes form (II) to form (III). The structure is twinned and the twinning operation is a 2₁ screw parallel to *a* using a symmetry operation that was present in form (II) and still exists on a local scale within the structure of form (III). Fig. 4(a) shows a schematic of the ribbon arrangement in form

Table 4

List of C11–H21... π distances (Å) for the three forms of benzocaine.

π is represented by the centroid position calculated from the atom positions of a six-membered ring.

Connectivity for molecules in the asymmetric unit	Form (I) ⁱ	Form (II) ⁱⁱ	Form (III)			
	1...1	1...1	1...2 ⁱⁱⁱ	2...1 ^{iv}	3...4 ⁱⁱⁱ	4...3 ^{iv}
D–H	0.99 (3)	0.959 (2)	1.00	1.00	1.00	1.00
H...A	2.82 (3)	3.1578 (1)	4.00	2.97	3.15	3.20
D...A	3.734 (3)	3.879 (2)	4.300 (4)	3.900 (4)	3.785 (4)	3.781 (4)
D–H...A angle (°)	153 (2)	133.3 (1)	101	155	123	118

Symmetry codes: (i) $1-x, 1-y, 1-z$; (ii) $\frac{1}{2}+x, 1-y, 1-z$; (iii) $2-x, \frac{1}{4}-y, \frac{1}{2}+z$; (iv) $1-x, \frac{3}{4}-y, z-\frac{1}{2}$. For (iii) and (iv) the transformation takes account of the origin shift used to draw Figs. 3, 4 and 5.

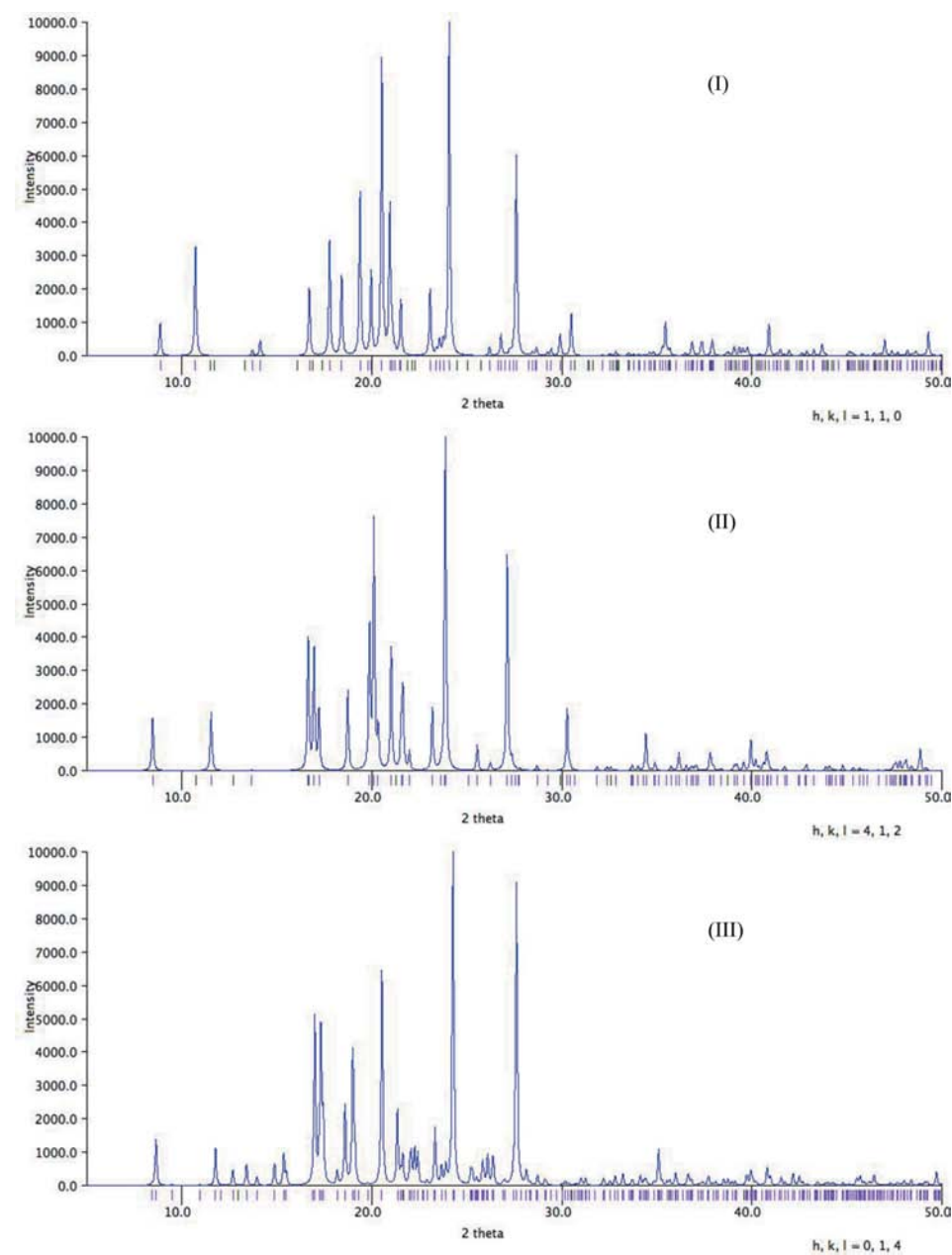


Figure 6 Powder diffraction patterns (Cu $K\alpha$) reconstructed from structures of the three forms for BZC.

(III). When the colour is the same the structure is essentially the same as form (II). When the colour changes the adjacent double-ribboned zigzag structure will have moved along **a**. As a consequence the interface between the twin components is probably also a zigzag. Using Fig. 4(a) we see that the local 2_1 screw between adjacent ribbons of the same colour in layers perpendicular to **c** can act as a twinning operation on that layer and when this occurs for every zigzag-related layer a different orientation of the structure exists on either side of the interface. Fig. 4(b) shows a projection down **c** of a layer of translation-related molecules perpendicular to **c*** for form (II). Fig. 4(c) shows a projection down **c** of two layers of molecules perpendicular to **c*** for form (III) that are related by a 2_1 screw axis parallel to **a**. Individual ribbons have local pseudo- 2_1 symmetry, which when projected down **c** look exactly the same as the interface between the layers shown in Fig. 4(c). The phase transition involves an anti-parallel translation of ribbons, as shown by the colours in Fig. 4(a). As a result the structure loses one in four of the N–H...N hydrogen-bonding interactions that were previously mentioned to exist in both form (I) and form (II). The one that is lost is replaced by a variety of new interactions with a N–H... π interaction the most striking, see Figs. 3 and 5, and Table 3. Now, sequences of zigzag ribbon-pair layer motifs related by the screw along **c** no longer stack with the screw parallel to **b***, creating continuous N–H...N hydrogen-bonded chains. Rather every fourth hydrogen bond is replaced by a newly formed N–H... π motif (Fig. 5). This results in a doubling of the **b**-axis repeat. Previous studies (Heinze & Reinhart, 2005; Bel'skii *et al.*, 1983) show that affinity for the centre of aromatic rings as hydrogen-bond acceptors is not uncommon, especially for nitrogen donors.

Values for $\text{CH}_3 \cdots \pi$ distances between parallel ribbons in the low-temperature form (Table 4) indicate that one in four of these interactions is greatly diminished because of the step between the zigzag bi-layers. The other three show a trend that is consistent with the fact that the three $\text{N}-\text{H} \cdots \text{N}$ interactions propagate in a line that is not strictly parallel to \mathbf{b}^* , as can be seen in Fig. 5, *i.e.* the molecules within a zigzag bi-layer are displaced to some extent to accommodate the sliding of the zigzag bi-layers perpendicular to \mathbf{b}^* . This prevents the γ angle of the unit cell from being even bigger.

A similar low-temperature phase transition for form (I) can be ruled out by a symmetry argument. The hydrogen-bonded interfaces between layers of ribbons are inversion-related in form (I) as opposed to screw-related in form (II). As a consequence, translating a single ribbon parallel to \mathbf{a} in form (II) creates $\text{N}-\text{H} \cdots \pi$ motifs on both edges of the ribbon with one edge providing donors, the other providing acceptors, see Fig. 3. Translating a ribbon parallel to \mathbf{a} in form (I) to create $\text{N}-\text{H} \cdots \pi$ motifs on one edge of the ribbon moves the molecules on the other edge in the opposite direction to that required.

Only every second ribbon on the outside of a zigzag bi-layer of form (III) is involved with the creation of $\text{N}-\text{H} \cdots \pi$ motifs, see Fig. 4(a). The two layers of a bi-layer are related by a 2_1 screw axis parallel to \mathbf{c} , as are adjacent bi-layers. Their relative positions determine the γ angle and create the remaining $\text{N}-\text{H} \cdots \text{N}$ interactions.

From the structures it is speculated that no solid–solid structural transformation can occur between form (I) and form (II). This assumption is based on the (I)–(II) transition requiring a mechanically unfavourable solid-state reconstruction of the crystal. If a transition were to occur, it could well involve a loss of material to a liquid or gaseous phase followed by re-crystallization. This speculation is contrary to thermodynamic arguments that have been put forward by Schmidt (2005a) and Gruno (Gruno *et al.*, 1993) using powder diffraction and differential scanning calorimetry to show that form (I) and form (II) are enantiotropically related. We suggest that the two forms could actually be monotropically related (Bernstein, 2002). To clarify this, re-constructed powder patterns (Macrae *et al.*, 2006) of the three forms are shown (Fig. 6) for comparison with those put forward by the above authors. The structural nature of the solid referred to as BZC mod II or BZC β described in the above literature is at variance with our interpretations, but the materials were formed under different conditions. It is reasonable to suggest that because of the great similarity between the hydrogen-bonded interfaces between adjacent layers of ribbons, intergrowths of forms (I) and (II) are possible. In rapidly formed crystals this would certainly degrade the quality of a powder diffraction pattern. The crystal structures obtained do not suggest that either form (I) or form (II) is the more stable at room temperature.

4. Conclusion

Form (II) of BZC undergoes a low-temperature phase transition to a new form (III), while form (I) does not. A phase transition between forms (I) and (II) is deemed unlikely based on structural considerations. It is speculated that solids containing components of all forms may well be possible and give possible mechanisms for twinning and disorder.

Future investigations will involve a more complete understanding of the nature of the mechanisms of the phase transition over a range of temperatures and further interpretation of the competition between interactions involved in all forms for the system. These will be strongly based on single-crystal X-ray diffuse scattering experiments at different temperatures. This will assist the identification of the temperature range for the phase transition and whether it is truly reversible.

The support of the Australian Research Council is gratefully acknowledged. The authors thank Dr Tony Willis of the Research School of Chemistry for assistance with the collection of Bragg data.

References

- Bel'skii, V. K., Rotaru, V. K. & Kruchinin, M. M. (1983). *Kristallografiya*, **28**, 695–698.
- Bernstein, J. (2002). *Polymorphism in Molecular Crystals*, pp. 29–42. Oxford University Press.
- Chan, E. J., Welberry, T. R., Goossens, D. J., Heerdegen, A. P., Beasley, A. G. & Chupas, P. J. (2009). *Acta Cryst.* **B65**, 382–392.
- Coppens, P. (1970). *Crystallographic Computing*, edited by F. R. Ahmed, S. R. Hall & C. P. Huber, pp. 255–270. Copenhagen: Munksgaard.
- Gruno, M., Wulff, H. & Pfliegel, P. (1993). *Pharmazie*, **48**, 834–837.
- Hall, S. R., du Boulay, D. J. & Olthof-Hazekamp, R. (2001). *XTAL3.7*. University of Western Australia, Perth.
- Heinze, K. & Reinhart, A. (2005). *Z. Naturforsch. B Chem. Sci.* **60**, 758–762.
- Hooft, R. (2005). *Collect. Nonius BV*, Delft, The Netherlands.
- Lynch, D. E. & McClenaghan, I. (2002). *Acta Cryst.* **E58**, o708–o709.
- Macrae, C. F., Edgington, P. R., McCabe, P., Pidcock, E., Shields, G. P., Taylor, R., Towler, M. & van de Streek, J. (2006). *J. Appl. Cryst.* **39**, 453–457.
- Otwinowski, Z. & Minor, W. (1997). *Methods in Enzymology*, edited by C. W. Carter & R. M. Sweet, pp. 307–326. New York: Academic Press.
- Rae, A. D. (1975a). *Acta Cryst.* **A31**, 560–570.
- Rae, A. D. (1975b). *Acta Cryst.* **A31**, 570–574.
- Rae, A. D. (2006). *RAELS2006*. Australian National University, Canberra.
- Schmidt, A. C. (2005a). *Int. J. Pharm.* **298**, 186–197.
- Schmidt, A. C. (2005b). *Pharm. Res.* **22**, 2121–2133.
- Sheldrick, G. M. (2008). *Acta Cryst.* **A64**, 112–122.
- Sinha, B. K. & Patabhi, V. (1987). *Proc. Indian Acad. Sci. Chem. Sci.* **98**, 229–234.